
Oral presentation | Incompressible/compressible/hypersonic flow

Incompressible/compressible/hypersonic flow-I

Wed. Jul 17, 2024 2:00 PM - 4:00 PM Room D

[8-D-03] Simulation of High Altitude Rarefied Hypersonic Flow with Large Species Density Variation Based on DSMC Method

*Takato Morimoto¹, Virgile Charton^{1,2}, Eiichiro Yamaoka¹, Kiyoshi Kinefuchi¹ (1. Department of Aerospace Engineering, Nagoya University, 2. Japan Society for the Promotion of Science International Research Fellow)

Keywords: Hypersonic flow, Rarefied flow, DSMC, Ionized flow

Simulation of High Altitude Rarefied Hypersonic Flow with Large Species Density Variation Based on DSMC Method

T. Morimoto*, V. Charton**, E. Yamaoka*, and K. Kinefuchi*

Corresponding author: kiyoshi.kinefuchi@mae.nagoya-u.ac.jp

* Department of Aerospace Engineering, Nagoya University, Japan

** Japan Society for the Promotion of Science International Research Fellow

Abstract: DSMC (Direct Simulation Monte Carlo) is a method widely used for solving rarefied flow, but it computes difficulty the trace species contained in weakly ionized plasmas. In this paper, two approaches are proposed to address this issue. The first method consists of decoupling the plasma computation from the flow computation using a post-processing chemical solver. The second method uses a species weighting scheme implemented in the DSMC code to increase the number of particles representing trace species. These two methods are applied to the OREX reentry flight and allow for the obtaining of a smooth electron number density field around the vehicle in the rarefied regime. The simulated values were compared with experimental measurements of electron number density. The overall results were consistent with the data trends.

Keywords: Hypersonic flow, Rarefied flow, DSMC, Ionized flow

1 Introduction

During vehicle re-entry into the atmosphere, aerodynamic heating causes air ionization in the high-temperature hypersonic flow field. The formed plasma sheaths can cause a disruption of communication between the vehicle and the control system, the so-called radio frequency blackout. Thus, precise electron number density field simulation is essential for predicting and preventing this issue. This phenomenon can occur at high altitude, where the Navier–Stokes equations solved in standard Computational Fluid Dynamics calculation (CFD) are not suitable for resolving rarefied gas. This paper focuses on the high altitude nonequilibrium rarefied plasma flow simulation to investigate the relationship between the plasma evolution behavior and the blackout onset. Thus, the DSMC (Direct Simulation Monte Carlo) method [1] is used, as it is a well-known stochastic method for simulating rarefied gases. DSMC uses numerical particles, each representing real molecules, and successively compute their trajectory and collisions. In the DSMC method, the number of particles employed is directly proportional to the total number density regardless of the chemical species. Thus, in the particular case of weakly ionized plasmas with significant number density changes among the species, an enormous number of particles of the most concentrated species is required to simulate the trace species, such as electrons, as they have a low concentration relative to others. This constraint leads to significant computation time and memory issues, preventing the obtaining of accurate electron number density fields.

In this study, this problem is addressed with two different approaches. The first is to post-compute the flow chemical composition by extracting the flow properties along the streamlines of a baseline DSMC simulation. This approach allows us to obtain a more precise flow composition, including trace species. It was proposed by Boccelli *et al.* [2] and developed in the Lagrangian chemical solver LARSEN. The second one proposes to use a species weighting scheme in the DSMC simulation, enabling the simulation of trace species by defining different ratios between the simulated particle and the real particles, using different numerical weights depending on their specie. Such a scheme is not available in the conventional DSMC code, as special care has to be given regarding the conservation of mass, momentum and energy. For this matter, a nonconservative scheme was first proposed by Bird [3]. Boyd

[4] then developed the split-merge method, which ensures the conservation of momentum and energy during the collision of differently weighted particles. Finally, species weighting schemes involving chemical reactions have been analyzed by Wu *et al.* [5], and Petkow *et al.* [6]. In the literature, a few cases of application of this method to hypersonic plasma have been shown [7,8].

This paper applies the post-computation and the species weighting scheme methods to the simulation of OREX (Orbital Reentry EXperiment) flight [9] conducted in 1994 to investigate the plasma development process during reentry. The results of the two methods are compared with the experimental data to evaluate their validity and discuss their limitations. This paper presents the following contents: Chapter 2 describes the flight case used for the simulations, Chapter 3 introduces the two methods used to resolve the trace species, including the scheme details and models used in the simulations, and Chapter 4 discusses the computational results and provides a comparison of the plasma flow fields.

2 Simulation Case

The OREX flight (Orbital Re-entry Experiment) conducted by NAL (National Aerospace Laboratory of Japan) and NASDA (National Space Development Agency of Japan) in 1994 was selected for the simulation case. During the flight, measurement of ion saturation current using electrostatic probes and observations of blackouts at multiple base stations were conducted, as well as aerodynamic heating data at different altitudes, including the rarefied atmosphere. In the work of Gupta *et al.* [10], these data were used to validate nonequilibrium chemical models. The Viscous Shock Layer (VSL) approach was also applied to the flight to reconstruct the boundary layer, as investigated by Doihara *et al.* [11]. The geometry of the OREX vehicle is shown in the Figure 1. The flight conditions simulated in this paper are those formerly simulated by Moss *et al.* [12], also employing DSMC. Simulations are performed for the four cases of flow conditions shown in Table 1. In the two low-altitude cases, the ion current is saturated and within the electron number density measurement range.

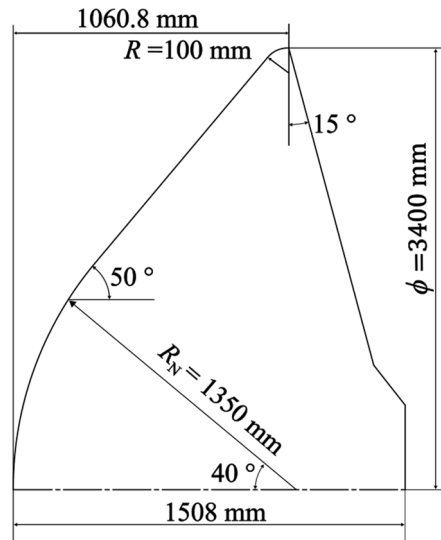


Figure 1: Geometry of OREX cross section

Table 1: Flow condition of simulated flight cases

	Altitude (km)	Velocity (m/s)	Temperature (K)	Number density (/m ³)	Knudsen number
(a)	105.0	7451	211.0	5.05×10^{18}	7.2×10^{-2}
(b)	101.1	7455	196.9	1.03×10^{19}	3.5×10^{-2}
(c)	96.8	7456	190.3	1.98×10^{19}	1.8×10^{-2}
(d)	92.8	7454	188.3	4.08×10^{19}	8.6×10^{-2}

Throughout the analysis, the air is modelled by an 11 chemical species representation ($N_2, O_2, NO, N, O, N^+, O^+, NO^+, N_2^+, O_2^+, e^-$) with the corresponding chemical reactions shown in Table 2. The forward reaction rate k_f is expressed in the modified Arrhenius form:

$$k_f = CT^\eta \exp(-\theta_d/T) \quad (1)$$

Where C is the pre-exponential factor, η is the temperature exponent, and θ_d is the characteristic temperature. The coefficients of all the reactions are listed in Table 2 [13], where M and A are the third body of the dissociation reactions (reactions 1-3), M being a diatomic molecule and A being a monatomic molecule (excluding electron).

Table 2: Reaction rate coefficients for high temperature air

No.	Reactions	C [cm ³ /(mol · s)]	θ_d [K]	η
1-a	$N_2 + M \rightarrow N + N + M$	7.00E+21	113200	-1.6
1-b	$N_2 + A \rightarrow N + N + A$	3.000E+22	113200	-1.6
2-a	$O_2 + M \rightarrow O + O + M$	1.000E+19	59500	-1.5
2-b	$O_2 + A \rightarrow O + O + A$	1.000E+19	59500	-1.5
3-a	$NO + M \rightarrow N + O + M$	1.100E+14	75500	0
3-b	$NO + A \rightarrow N + O + A$	1.100E+14	75500	0
4	$NO + O \rightarrow N + O_2$	8.40E+12	19450	0
5	$N_2 + O \rightarrow NO + N$	6.40E+17	38400	-1
6	$N + O \rightarrow NO^+ + e^-$	8.80E+08	31900	1
7	$O + O \rightarrow O_2^+ + e^-$	7.10E+02	80600	2.7
8	$N + N \rightarrow N_2^+ + e^-$	4.40E+07	67500	1.5
9	$NO^+ + O \rightarrow N^+ + O_2$	1.00E+12	77200	0.5
10	$N^+ + N_2 \rightarrow N_2^+ + N$	1.00E+12	12200	0.5
11	$O_2^+ + N \rightarrow N^+ + O_2$	8.70E+13	28600	0.14
12	$O^+ + NO \rightarrow N^+ + O_2$	1.40E+05	26600	1.9
13	$O_2^+ + N_2 \rightarrow N_2^+ + O_2$	9.90E+12	40700	0
14	$O_2^+ + O \rightarrow O^+ + O_2$	4.00E+12	18000	-0.09
15	$NO^+ + N \rightarrow O^+ + N_2$	3.40E+13	12800	-1.08
16	$NO^+ + O_2 \rightarrow O_2^+ + NO$	2.40E+13	32600	0.41
17	$NO^+ + O \rightarrow O_2^+ + N$	7.20E+12	48600	0.29
18	$O^+ + N_2 \rightarrow N_2^+ + O$	9.10E+11	22800	0.36
19	$NO^+ + N \rightarrow N_2^+ + O$	7.20E+13	35500	0
20	$N + e^- \rightarrow N^+ + e^- + e^-$	3.90E+33	158500	-3.78
21	$O + e^- \rightarrow O^+ + e^- + e^-$	2.50E+34	168600	-3.82

Assuming a small angle of attack allows us to perform two-dimensional axisymmetric simulations. The computational domain was set at 5 m from the axis in the radial direction, 2 m (3 m only at an altitude of 105 km) upstream from the tip of the plane in the axial direction to capture thick shock waves, and 10 m downstream in the axial direction.

3 Numerical Method

3.1 Direct Simulation Monte Carlo

The DSMC (Direct Simulation Monte Carlo) method computes the behavior of a flow field by representing real flow molecules with numerical particles and calculating their trajectories and collisions at each timestep. Specifically, particle motions are first calculated according to their velocities

regardless of possible interactions. Then, collisions are resolved between nearby particles on a stochastic approach. The macroscopic flow quantities are obtained from the particles' microscopic quantities averaged over many timesteps. To accurately capture the flow of multi-species systems, it is necessary to set the time step smaller than the mean collision time between two particles, the cell size smaller than their mean free path and to use a sufficient number of numerical particles, from 10 to 20 per cell for each species.

The present simulation case is a weakly ionized plasma with trace species, such as electrons, having a mole fraction of less than 0.5%. It is not feasible to obtain the electron number density field while satisfying the above-described numerical conditions, especially regarding the number of particles per cell, as the number of the major species would significantly increase, leading to an unbearable computational effort. Therefore, in this study, the conventional DSMC method is only used in the plasma post-computation method scope to obtain the baseline aerodynamic characteristics of the flow. The computational code used is the open-source code SPARTA [14] (version 18 July 2022), made by Sandia National Laboratories under the GNU Public License. SPARTA features orthogonal grid simulations, allowing axisymmetric cases, using Bird [1] No Time Counter (NTC) algorithm to perform the particle collision. Figure 2 shows the computation grid of this study, obtained with an adaptive mesh refinement to ensure a correct spatial discretization regarding the particles' mean free path. Due to the extremely small mass of electrons, 1/1000 of the heavier particles, they are characterized by a large velocity compared to other particles. Consequently, the simulation of electrons requires a very small time step, which is not affordable. Therefore, the ambipolar approximation model is used [15], assuming ions and electrons move together while maintaining charge quasi-neutrality. The electron particles are then accounted for only in the collision calculations. The TCE (Total Collision Energy) model computes reaction occurrences, incorporating the modified Arrhenius equation into molecular units as in Table 2. Only neutral species are considered as third body for dissociation reactions (Table 2, reactions 1-3). Reverse reactions are considered for the exchange reactions [7] (Table 2, reactions 4, 5, 9-19). Energy distribution during collisions is modeled by the Borgnakke-Larsen model, and the collision model is set to the VSS (Variable Soft Sphere) model. Simulated energy modes include translational, rotational, and vibrational modes. For the vibrational relaxation rate model, the Millikan-White model with a high temperature correction [16] is implemented into the code and used during the simulations, and the Parker model is used for the rotational relaxation rate model [17]. The radiation phenomenon is not considered, and the vehicle wall is assumed to be a non-catalytic wall.

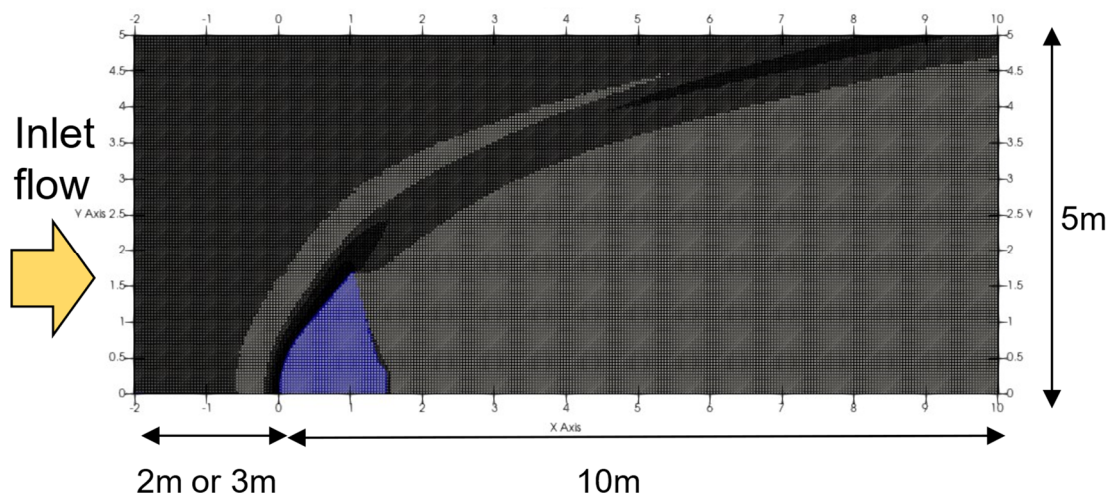


Figure 2: Example of calculated field setup. Adapted DSMC grid, with blue areas indicating body of the vehicle.

3.2 Method 1: Post-computation of detailed chemistry

The LARSEN solver developed by Boccelli *et al.* [2] is used to post-compute the plasma from the conventional DSMC solution. This post-computation approach allows the decoupling of the flow and the chemistry simulation to include complexity or more detailed thermochemical effects into a lower-

fidelity baseline solution using the thermochemical library Mutation++ [18]. Physical quantities (density, velocity, temperature, chemical species composition) are extracted along the streamlines, and the mass and energy equations are re-computed to give a more detailed chemical composition from one node of the streamline to another, assuming that the velocity and the density remain unchanged. This assumption is ensured by the negligible influence of the trace species on the flow momentum and enthalpy, allowing the extension of the chemistry to account for plasma reactions without affecting the flow velocity and density. However, the diffusion of mass and heat among the streamlines is not accounted for in LARSEN computation, and the new solution is integrated along every streamline separately. Thus, the wall influence is not accurately simulated in this approach.

A two-temperature model considering translational-rotational and vibrational-electronic excitation modes is used for the energy conservation equation. The enthalpy conservation in the translational-rotational mode is expressed in the Lagrange differential form as:

$$\frac{Dh^t}{Dt} = \left[Q - \frac{D(u^2/2)}{Dt} - \sum_i \frac{h_i \dot{\omega}_i}{\rho} - \left(\Omega_i^{in} - \sum_i \frac{h_i^{in} \dot{\omega}_i}{\rho} \right) \right] \quad (2)$$

Here, u is the flow velocity, and ρ is the mass density, both obtained from DSMC calculation results. h^t represents enthalpy. $\dot{\omega}_i$, h_i , h_i^{in} and Ω_i^{in} are the production rate of heavy particle chemical species i , production enthalpy, vibrational mode enthalpy, and energy exchange between modes, respectively. Q represents the change in enthalpy at each node calculated from DSMC results and is expressed in equation (3). It is introduced to correct the energy exchange between streamlines.

$$Q = \left(\frac{DH}{Dt} \right)_{ref} = \left(\frac{Dh^t}{Dt} + \frac{Dh^{in}}{Dt} + \frac{D(u^2/2)}{Dt} \right)_{ref} \quad (3)$$

Energy conservation in the vibrational mode is expressed similarly to equation (2). Finally, the translational temperature T is calculated at each node by using the mass fraction Y_i of species i and the specific heat of the translational mode $c_{p,i}^t$, as shown in equation (4).

$$\frac{DT}{Dt} = \frac{Dh^t}{Dt} / \left(\sum_i Y_i c_{p,i}^t \right) \quad (4)$$

LARSEN post-computation uses the chemical reaction coefficients shown in Table 2, computing the backward coefficient for all the reactions. For the thermodynamic model, the RRHO (Rigid Rotor Harmonic Oscillator) approach is employed. As in DSMC simulations, the vibrational relaxation rate are computed by the Millikan-White model with corrections for high temperatures, as proposed by Park [16]. Streamlines are obtained by uniformly taking 100 starting points from the inflow section of the flow computed by the conventional DSMC as described in the previous section.

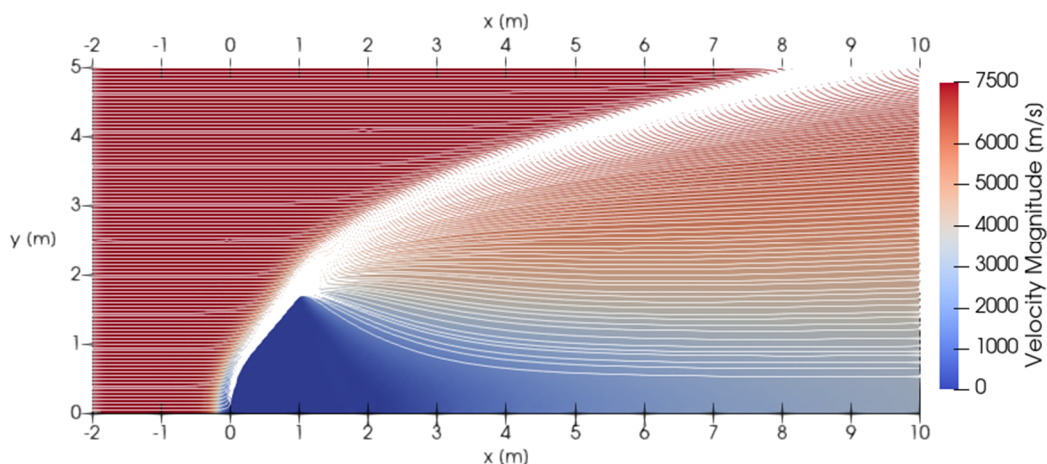


Figure 3: Extracted streamlines from DSMC result. LARSEN post-computation is applied to each one of them.

3.3 Method 2: Species weighting scheme

This method requires the implementation of a specific collision scheme in the code SPARTA, and therefore, more effort to set than the previous method. However, it has the advantage of obtaining the electron density field using a single simulation, the DSMC simulation, compared to the additional use of a chemical post-computation tool. In this method, each species i is assigned with a weight w_i so that all particles of the same chemical species have the same weight. This weight varies between 0 and 1 and modify the number of physical particles represented by the numerical particle. The final number of physical particles represented by a numerical particle is then given by the product of the global ratio of physical particles to simulated particles, F_N , multiplied by the weight w_i . The conventional DSMC is equivalent to have $w_i = 1$ for all the species. Setting low w_i lead to smaller product $w_i F_N$, hence fewer physical particles will be contained into each numerical particle of specie i , which means that more numerical particles will be employed in the DSMC computation to obtain the same number of physical particles. Therefore, setting low weights for trace species allows for an increase in the numerical particles of these species. For this reason, the species weighting scheme is typically introduced in systems with significant number density variation. While this resolves differences among species numerical particle concentration, it necessitates additional considerations in particle-pair selection, momentum, and energy conservation in addition to the conventional DSMC. Furthermore, due to chemical reactions, special attention to mass conservation is also required.

3.1.1 Collision number

Firstly, the modifications regarding inter-particle collisions are described in this section. In the classical NTC model, the number of collision pairs selected in a time step Δt is determined by the number of molecules represented by one particle F_N , the number of numerical particles N , the time step Δt , the collision cross section σ_t , and the relative velocity g_r of the colliding particles:

$$\frac{1}{2} N N F_N (\sigma_t g_r)_{max} \Delta t / V_{cell} \quad (5)$$

When species weighting is introduced, the number of real molecules in a cell is expressed as $F_N \sum_j w_{i,j} / V_{cell}$ by summing each particle j weighing factor $w_{i,j}$. Therefore, the modified number of collision pairs is represented as follows:

$$\frac{1}{2} N F_N (\sigma_t g_r)_{max} \Delta t \sum_j w_{i,j} / V_{cell} \quad (6)$$

After the NTC algorithm computes the number of collision pairs, the candidate particles are selected randomly across the cell particles. Each formed pairs is tested with an acceptance-rejection method according to the collision probability P_c , depending on the particle cross section and relative velocity. P_c is expressed as:

$$P_c = \frac{\sigma_t g_r}{(\sigma_t g_r)_{max}} \quad (7)$$

Although the number of collisions does not correspond to the real number of collisions, particle pairs with the higher $\sigma_t g_r$ product will more likely be selected to perform the collision, ensuring an accurate representation of the flow behavior. When using the species weighting scheme, the number of numerical particles is no longer proportional to the mixture composition. As the pair candidate selection is a random process, it can lead to selecting much more trace species for collisions compared to conventional DSMC. Even if these trace species collisions involve fewer physical particles due to their low weight, a careful balance between the number of numerical particles representing the trace species and the major species should be respected. Boyd [4] recommends using the species weighting scheme only for species having less than 0.1 mole fraction, and that the ratio of the weights of trace and major species to be chosen to be approximately equal to the ratio of their mole fractions.

3.1.2 Momentum and energy conservation

Secondly, the conservation of momentum and energy by the split-merge method [4] is explained in one dimension. Figure 4 illustrates the steps of the split-merge method when particles with different weights collide. Consider the collision of a particle a , representing species A having the weight w_A , with a particle b representing species B having the weight w_B . The masses of the molecules represented by the particles are m_A and m_B , respectively, and the pre-collision velocities of the particles are u_a and u_b . When $w_A > w_B$, i.e., when B is a trace species, we set the weight ratio as $\phi = w_B/w_A$. The collision momentum p_m is then expressed as follows:

$$\begin{aligned} p_m &= F_N w_A m_A u_a + F_N w_B m_B u_b \\ &= F_N w_A (m_A u_a + \phi m_B u_b) \end{aligned} \quad (8)$$

The split approach consists of taking only $\phi_B = F_N w_B$ physical particles from the particle a , having $\phi_A = F_N w_A$ physical particles, to actually collide and exchange energy with the particle b . The remaining physical particles of a , $\phi_A - \phi_B = F_N (w_A - w_B) = F w_A (1 - \phi)$, do not collide. Taking this into account, equation 8 is modified as follows:

$$p_m = F_N w_A \{(1 - \phi) m_A u_a + \phi (m_A u_a + m_B u_b)\} \quad (9)$$

The collision of a and b equivalent number of physical particles $F_N w_A \phi$ is processed by the Larsen-Borgnakke method, as in the conventional DSMC, resulting in the post-collision velocities u_a^* , u_b^* . Hence, the collision momentum:

$$p_m = F_N w_A \{(1 - \phi) m_A u_a + \phi (m_A u_a^* + m_B u_b^*)\} \quad (10)$$

The final step is to merge the split particle a to obtain the final post collision velocity u_a^{**} . To conserve momentum through the collision process, equation 11 should be respected:

$$p_m = F_N w_A m_A u_a^{**} + F_N w_B m_B u_b^* \quad (11)$$

Leading to the following expression of u_a^{**} , explicitly respecting the momentum conservation:

$$u_a^{**} = (1 - \phi) u_a + \phi u_a^* \quad (12)$$

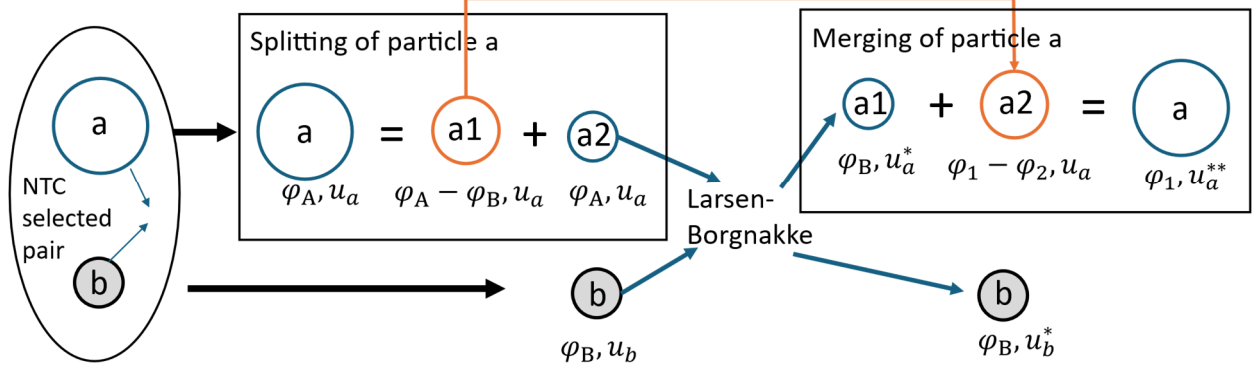


Figure 4: Split-merge model applied to the collision of particles a and b having respectively u_a and u_b velocities, and representing ϕ_A and ϕ_B number of physical particles with $\phi_A > \phi_B$. The post collision properties are denoted with the symbol $*$, and the merged particle with the symbol $**$

However, while this method conserves momentum, it does not conserve translational energy. The translational energy before the collision E_{pre} and after the collision E_{post} are given by:

$$E_{pre} = F_N w_A \frac{1}{2} m_A u_a^2 + F_N w_B \frac{1}{2} m_B u_b^2 \quad (13)$$

$$E_{post} = F_N w_A \frac{1}{2} m_A u_a^{*2} + F_N w_B \frac{1}{2} m_B u_b^{*2} \quad (14)$$

The difference in these energies is:

$$\Delta E = F_N w_A \frac{1}{2} m_A \phi (1 - \phi) (u_a - u_a^*)^2 \quad (15)$$

Note that for $w_A = w_B$, $\phi = 1$ and $\Delta E = 0$, so that energy is conserved exactly when the weights of the two particles are equal. If the split-merge scheme is employed at each collision, then energy is continually lost from the system because $\Delta E > 0$. This problem is addressed by keeping track of these energy losses in each cell. Then, when one collision loses energy through equation 15, this energy is then added to the energy of a subsequent collision. In general, this energy should only be added to collisions between particles having the maximum weight used in the simulation; that is, between two major particles (leading to a non-trace collision). The energy addition is performed by increasing the relative velocity of the next non-trace collision to make up the energy lost in the previous split-merge collision. In this manner, the maximum energy lost is only that caused by a single collision. When it is noted that the magnitude of ΔE is proportional to ϕ , it becomes clear that the amount of energy lost is very small, and particularly so for those species present in very small amounts for which ϕ is itself very small. The amount of energy to be added to the next non-trace collision is a variable maintained in each cell of the simulation. Whenever several collisions occur sequentially in which $w_A \neq w_B$ (i.e., the split-merge procedure is employed), then the energy to be made up for each of these collisions is summed until a non-trace collision occurs. Thus, energy conservation is maintained over all iterations of the simulation.

3.1.3 Chemical reactions

Thirdly, chemical reactions with species weighting are described in this section. In a conventional DSMC case, when two particles collide and the TCE algorithm determines that a reaction is occurring, two or three product numerical particles are created, depending on the reaction type. The mass is automatically conserved as the colliding and the product particles represent the same number of physical particles. However, when using the species weighting scheme, special consideration is required due to the different weights of the reactant and product particles. Based on the split-merge method, only the amount corresponding to the particle with the smaller weight reacts and the same amount of product is created. Thus, in every possible reaction scenario, involving minor and major species as reactant and/or product, the final number of created particles depends on the smallest weight that is involved in the process. Assume that particle c representing a product specie C is created from the collision and reaction between particle a and trace species particle b . Let the smallest weighting factor among the reactant particles be $w_{r,min}$. In this example, $w_{r,min} = w_B$, and $F_N w_{r,min}$ molecules are involved in the reaction. The process of product creation changes based on the ratio between $w_{r,min}$ and w_C .

- i) If $w_C/w_{r,min} < 1$:
The number of physical particles represented by the particle c is less than the number of physical particles involved in the reaction, so the particle c are multiplied to create w_C/w_{min} particles.
- ii) If $w_C/w_{r,min} > 1$:
The number of physical particles represented by the particle c is, this time, higher than the number of physical particles involved in the reaction. Thus, creating one c particle will overestimate the number of physical particles of species C. Therefore, when this reaction occurs, the particle c is created with a probability of $w_{r,min}/w_C$. Otherwise, it is not created.

Regarding the reactants, part of the physical particles contained in one of the two numerical particles might not react. Let the largest weighting factor of the reactants be $w_{r,max}$. When the collision occurs, physical particles of the major specie corresponding to $(w_{r,max} - w_{r,min})$ do not participate in the

reaction. Therefore, the particle representing the non-minor specie should partly remain in the cell after the reaction. To satisfy mass conservation, the reactant particle with the higher weight remains after the reaction with a probability of $(w_{r,max} - w_{r,min})/w_{r,max}$ and is deleted otherwise.

The above method was implemented in SPARTA in the scope of this work. Momentum, energy and mass conservation were validated by a single-cell close system case. For the OREX simulation case using the species weighting scheme, the same physical properties and model as described in section 3.1 are used. The weighting factor for neutral particles is set to $w_i = 1$. The weighting factor for ions and electrons, having a maximum mole fraction around $1e-4$ and thus considered as trace species, is set to $w_i = 0.01$. Ions and electrons have the same weights to satisfy charge conservation.

3 Results and Discussion

3.1 Temperature comparison and shock wave analysis

The results obtained by the two methods are presented in this section and compared to conventional DSMC in order to confirm their validity in regard to the shock physics. Firstly, Figure 5 shows the temperature field obtained by the baseline DSMC calculation and after LARSEN re-computation to visualize the influence of chemistry post-computation. The lower part represents the DSMC translational temperature field, while the upper part represents the reconstructed translational temperature field. In terms of flow field characteristics, the shock wave thickness increases as the mean free path of the flow increases. In other words, the more rarefied the flow is, the thicker the shock wave becomes. This observation agrees with the expectation of rarefied flow shock wave behavior.

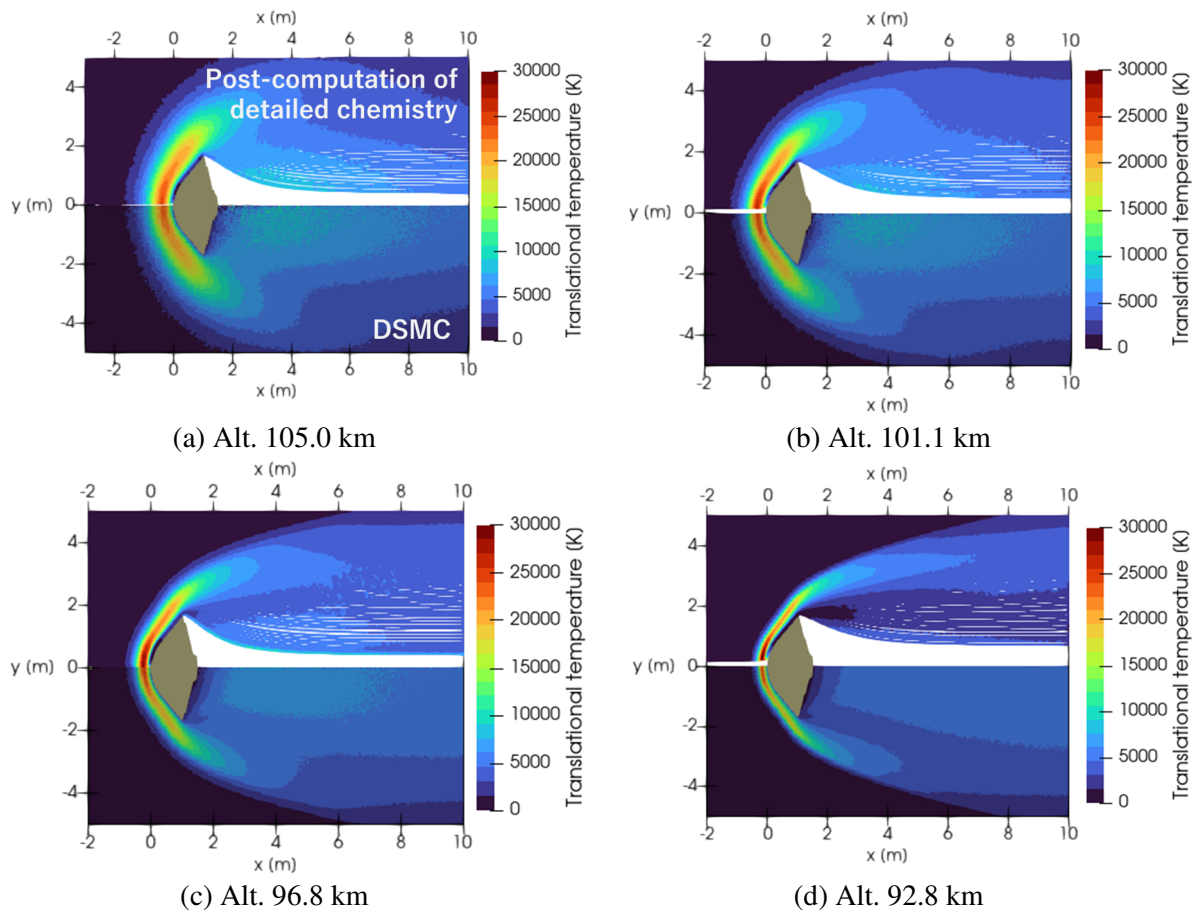


Figure 5: Translational temperature field comparison between LARSEN post-computation of detailed chemistry (upper) and DSMC (lower)

Generally, the characteristics of the flow field have not changed between the conventional DSMC and LARSEN, which validate the use of the post-computation approach assuming negligible change in density, velocity and enthalpy of the flow. Specifically, the thick shock wave characteristic of rarefied flows remains unchanged. However, slight changes in the temperature field behavior at the rear of the flow can be observed. Furthermore, at the lowest altitude (d), the temperature behind the shock wave is particularly different. To analyze the results in further detail, the temperature profile along a streamline starting from the front inlet boundary and at a height of 0.2 meters from the axis is shown in Figure 6. There is no change in the rising and peak positions of the translational temperature. However, differences can be seen in the absolute value of the translational temperature and the peak position of the vibrational temperature. A possible reason for this difference is that the rotational temperature is independently modeled in DSMC, whereas LARSEN employs a two-temperature modeling (translational and vibrational). Thus, the forms of energy transport might not perfectly match. Moreover, the delayed peak in vibrational temperature can result from the streamline post-computation approach inability to account for the wall effects, which is modeled as an isothermal wall.

Secondly, the second method temperature fields are confronted with conventional DSMC in Figure 7. Almost no change in the shock wave temperature is observed when using the species weighting scheme. However, differences are observed in the wake, which can be caused by a relative reduction in the number of major species numerical particles due to weighing, as the total number of numerical particles used with and without species weighting is fixed. Globally, the two methods lead to the correct simulation of the rarefied shock behavior, and both approaches results for electron number density are presented in the next section.

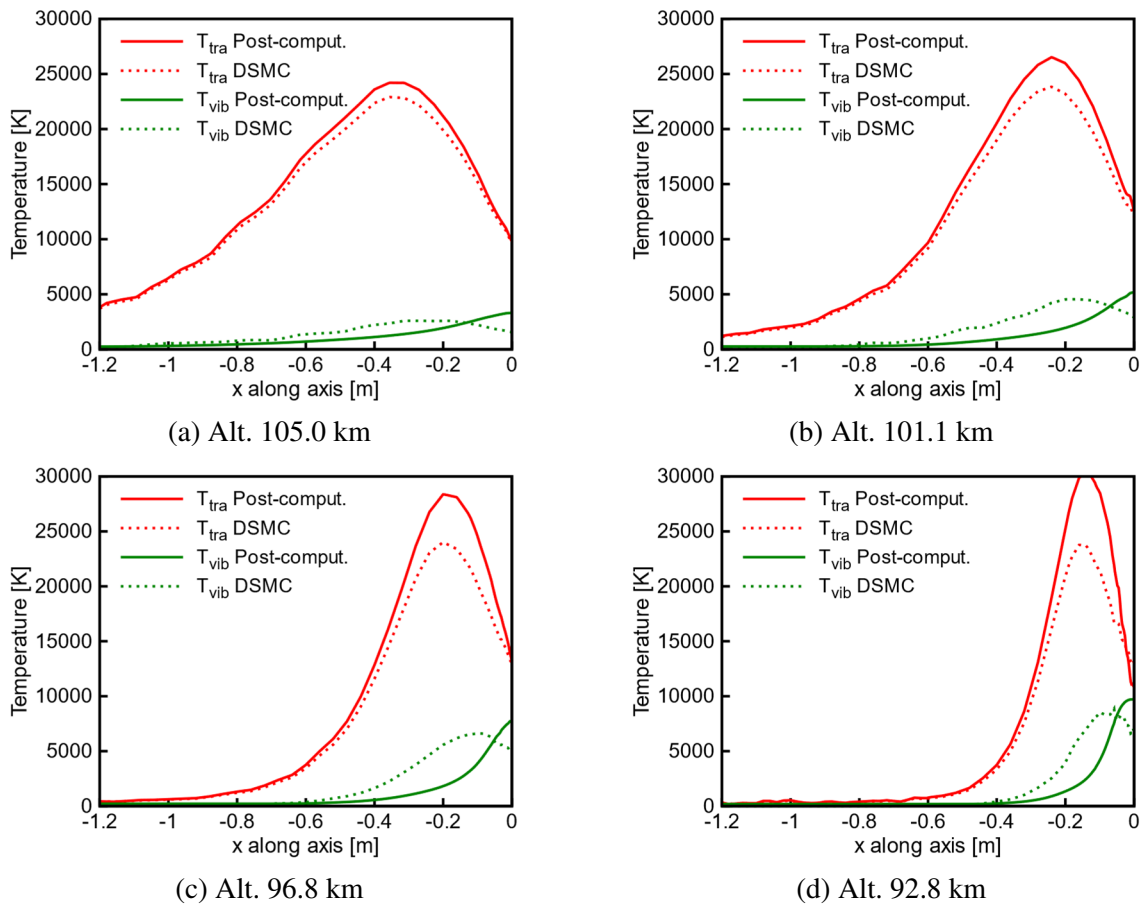


Figure 6: Translational temperature T_{tra} and vibrational temperature T_{vib} of the shock wave along the streamline starting from the front inlet and at a height of $y = 0.2$ m away from the axis. The solid lines show post-computation results and the dotted line shows the DSMC-only results.

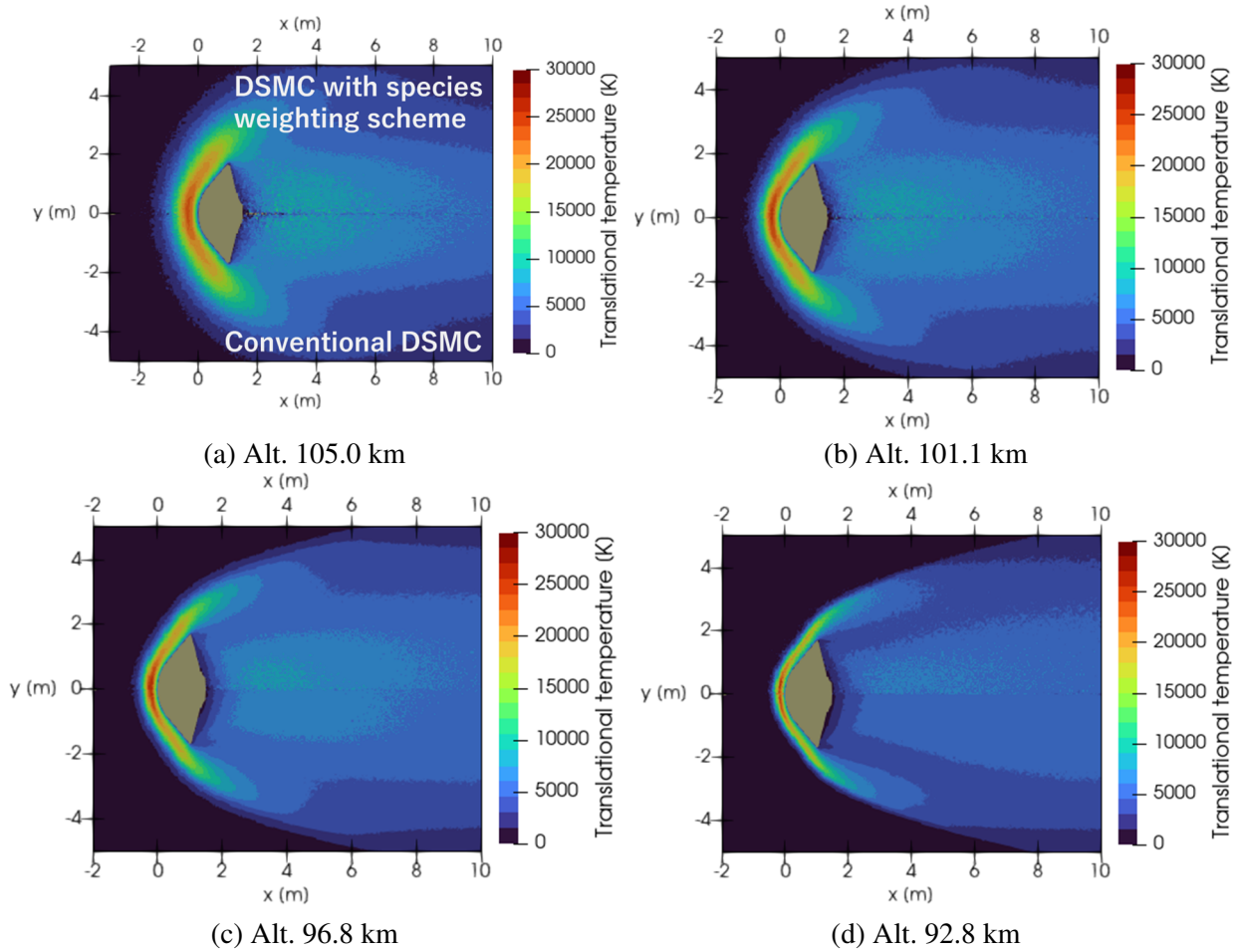


Figure 7: Translational temperature field comparison of DSMC results using species weighing scheme (upper) and conventional DSMC (lower)

3.2 Comparison of electron number density

The electron distributions obtained with LARSEN post-computation and with the species weighting scheme approaches are presented in Figure 8 for the four studied altitudes. As the same weight settings are used for all the species weighting scheme simulations, the electron particle resolution decreases for the high-altitude cases (a) and (b) as the rarefaction increases. However, the electron density number is smooth enough behind the shock for all the simulations, which is the region of interest of this study as it is where the OREX electrostatic probe is localized. The results of the two methods show similarly produced electrons behind the shock and around the edges of the OREX vehicle. However, for the lowest altitude, the electron number density behind the body is higher when simulated with the species weighting scheme approach. This discrepancy can be due to the backward reaction of the ionization reaction being incorporated in the post-computation method, whereas the species weighting scheme does not account for them. This explanation goes along with the fact that the difference arises for the lowest altitude case when the flow density increases and thus the potential number of collisions and reactions that would lead to electron recombination.

Figure 9 compares the simulation results and the flight measurements taken by the electrostatic probe localized at 943.5 mm axially and 1626.2 mm radially from the body tip. The probe acquires in-flight ion saturation currents. To deduce the electron number density from it, CFD computation of the flow was performed to estimate electron temperature.[9]. Figure 9 displays the flight electron density reconstructed from the probe data using CFD with the one temperature model, denoted as 1-temp, and two temperature model, denoted 2-temp. The trend in the electron density evolution with altitude is consistent between the two methods and the flight data. However, some discrepancies are observed.

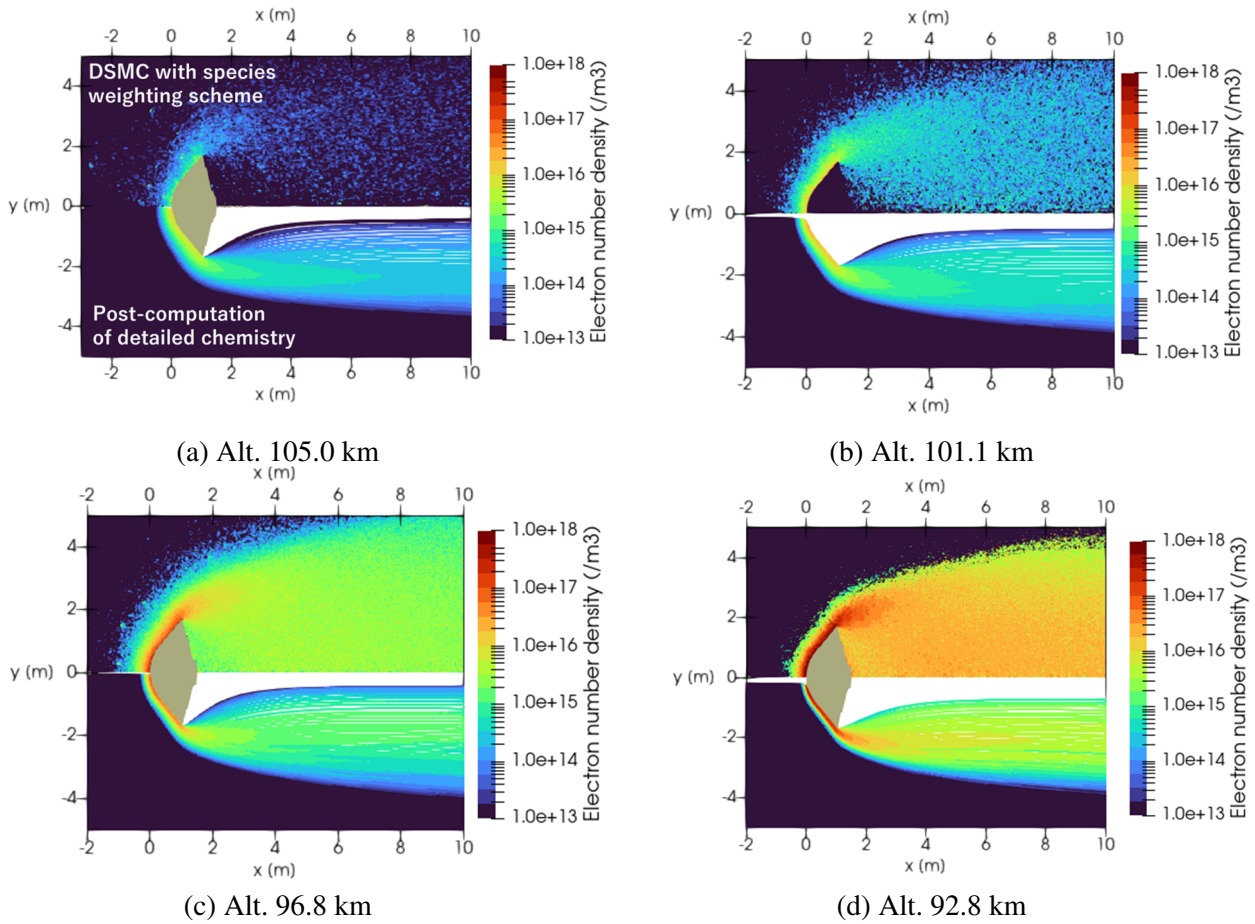


Figure 8: Comparison of electron number density distributions using the species weighing scheme (upper) and the detailed chemical post-computation (lower) for the four studied altitudes

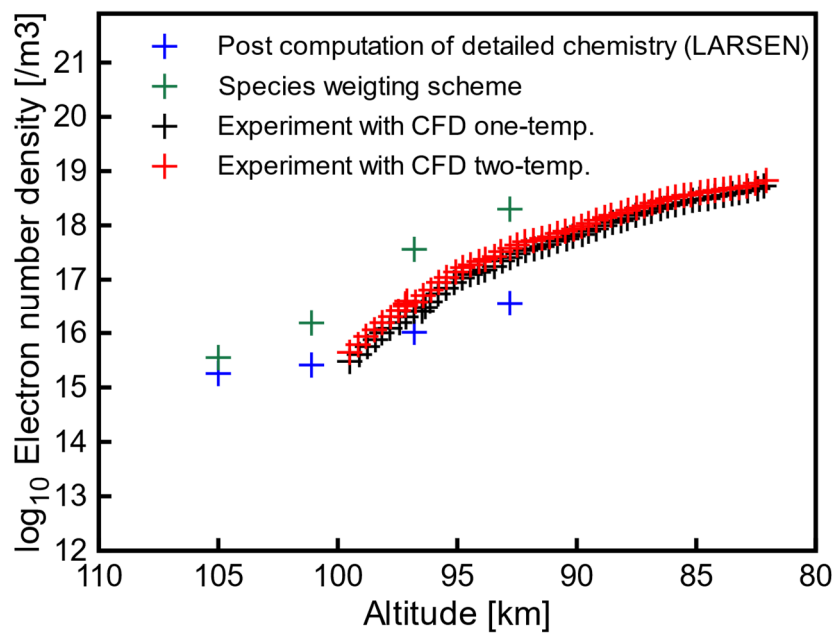


Figure 9: Comparison of electron number density obtained with the two methods described in this work with the experimental probe data

Firstly, the results obtained with the species weighing scheme show an overestimation of the electron number density for all the simulated altitudes. As previously mentioned, one of the reasons that can explain this result is that the backward ionization reactions were not considered (reactions 6 to 8) when using the species weighting scheme as the handling of weighted electron recombination is very difficult and requires additional efforts. In addition, the catalyst characteristic of the wall is not modelled in the present calculation, which can also influence the electron density. This last point should be further investigated in future work, as it was accounted in Moss *et al.* [12] study on the same configuration. Secondly, the post-computation approach underestimates the electron number density, especially at low altitudes. With this method, the ionization backward reactions are taken into account, which can explain the decrease in the electron number density. Furthermore, the wall interaction is not modelled, and it is difficult to estimate its influence on the electron number density in the probe area. Finally, both methods provided high-resolution electron number density field, which is hardly achievable using conventional DSMC, and reproduced the tendency observed during the flight experiment.

4 Conclusion

In this study, two approaches were used to obtain the distribution of electrons in simulations of high-altitude dilute hypersonic flows with significant variations in species density. These approaches, a post-computation of detailed chemistry using a Lagrangian solver and the implementation of a species weighting scheme in DSMC, were applied to the OREX experiment case. The data measured during the flight experiment were used to discuss the validity of the two approaches for different altitudes. Both methods provided the trace species number density field around the OREX vehicle, including the electrons. Such simulation of the trace species is hardly feasible with conventional DSMC codes and significantly improves the analysis of the plasma generation and behavior during high altitude hypersonic flow. Both methods confirmed similar trends compared to the experimental data, especially in the electron number density. However, discrepancies in the temperature profiles and underestimation of the electron number density at low altitudes were observed when using the post-calculation method. This can be explained by the difference in the energy transport modeling and by the wall influence and mass and heat diffusion that is not accounted for in the streamline post-computation approach. On the other hand, the species weighting scheme overestimated the electron density profile in some regions. This can be attributed to the backward ionization reaction that is not yet handled by the species weighting scheme due to its complexity. A future work will be to implement these backward reactions and assess their impact on the flow ionization. Overall, this study highlights the potential of these methods, allowing us to obtain a high-resolution solution of plasma trace species, improving the accuracy and efficiency of hypersonic plasma flow simulations involving high variation among the flow species.

Acknowledgments

This work was supported by the grant from Sumitomo Electric Industries CSR Foundation. Part of the computer simulation was performed on the KDK computer system at Research Institute for Sustainable Humanosphere, Kyoto University.

References

- [1] Bird GA. *Molecular Gas Dynamics and the Direct Simulation of Gas Flows* (Oxford Engineering Science Series). Oxford University Press; 1994.
- [2] Boccelli S, Dias B, Magin TE. Lagrangian diffusive reactor for detailed thermochemical computations of plasma flows. *Plasma Sources Sci Technol* 2019;28:065002. <https://doi.org/10.1088/1361-6595/ab09b5>.
- [3] Bird GA. *Molecular Gas Dynamics*. Clarendon Press; 1976.

- [4] Boyd ID. Conservative Species Weighting Scheme for the Direct Simulation Monte Carlo Method. *Journal of Thermophysics and Heat Transfer* 1996;10:579–85. <https://doi.org/10.2514/3.832>.
- [5] Wu J-S, Hsiao W-J, Lian Y-Y, Tseng K-C. Assessment of conservative weighting scheme in simulating chemical vapour deposition with trace species. *International Journal for Numerical Methods in Fluids* 2003;43:93–114. <https://doi.org/10.1002/flid.609>.
- [6] Petkow D, Mirza A, Herdrich G, Fasoulas S. Treatment of differently weighted particles in reactive re-entry flows with DSMC, Zaragoza, Spain: 2012, p. 1507–14. <https://doi.org/10.1063/1.4769717>.
- [7] Boyd ID. Modeling of associative ionization reactions in hypersonic rarefied flows. *Physics of Fluids* 2007;19. <https://doi.org/10.1063/1.2771662>.
- [8] Fang M, Li Z-H, Li Z-H, Liang J, Zhang Y-H. DSMC modeling of rarefied ionization reactions and applications to hypervelocity spacecraft reentry flows. *Adv Aerodyn* 2020;2:1–25. <https://doi.org/10.1186/s42774-020-00030-1>.
- [9] Inouye Y. OREX flight - quick report and lessons learned. *Aerothermodynamics for space vehicles, Proceedings of the 2nd European Symposium, Noordwijk, The Netherlands: 1995*, p. 271.
- [10] Gupta RN, Moss JN, Price JM. Assessment of Thermochemical Nonequilibrium and Slip Effects for Orbital Re-Entry Experiment. *Journal of Thermophysics and Heat Transfer* 1997;11:562–9. <https://doi.org/10.2514/2.6280>.
- [11] Doihara R, Nishida M. Thermochemical nonequilibrium viscous shock layer studies of the orbital reentry experiment (OREX) vehicle. *Shock Waves* 2002;11:331–9. <https://doi.org/10.1007/s001930200119>.
- [12] Moss JN, Gupta RN, Price JM. DSMC simulations of OREX entry conditions. *Rarefied Gas Dynamics*, Beijing: Peking University Press; 1996, p. 459–64.
- [13] Park C. Review of chemical-kinetic problems of future NASA missions. I - Earth entries. *Journal of Thermophysics and Heat Transfer* 1993;7:385–98. <https://doi.org/10.2514/3.431>.
- [14] Plimpton SJ, Moore SG, Borner A, Stagg AK, Koehler TP, Torczynski JR, et al. Direct simulation Monte Carlo on petaflop supercomputers and beyond. *Physics of Fluids* 2019;31. <https://doi.org/10.1063/1.5108534>.
- [15] Bird G. Nonequilibrium radiation during re-entry at 10 km/s. 22nd Thermophysics Conference, American Institute of Aeronautics and Astronautics; 1987. <https://doi.org/10.2514/6.1987-1543>.
- [16] Park C. Nonequilibrium hypersonic aerothermodynamics. Wiley; 1989.
- [17] Parker JG. Rotational and Vibrational Relaxation in Diatomic Gases. *Phys Fluids* 1959;2:449–62. <https://doi.org/10.1063/1.1724417>.
- [18] Scoggins JB, Leroy V, Bellas-Chatzigeorgis G, Dias B, Magin TE. Mutation + + : MULTicomponent Thermodynamic And Transport properties for IONized gases in C++. *SoftwareX* 2020;12:100575. <https://doi.org/10.1016/j.softx.2020.100575>.
- [19] Boyd ID, Schwartzenuber TE. *Nonequilibrium Gas Dynamics and Molecular Simulation*. Cambridge University Press; 2017.
- [20] Zhang W, Zhang Z, Wang X, Su T. A review of the mathematical modeling of equilibrium and nonequilibrium hypersonic flows. *Adv Aerodyn* 2022;4:1–47. <https://doi.org/10.1186/s42774-022-00125-x>.